

Photoelectrochemical behavior of WO_3 and TiO_2 films modified with cobalt-based oxygen evolution catalyst

Simona Ostachavičiūtė*,

Rasa Mardosaitė,

Eugenijus Valatka

*Department of Physical
and Inorganic Chemistry,
Kaunas University
of Technology,
Radvilėnų Rd. 19,
LT-50254 Kaunas,
Lithuania*

Continuous tungsten trioxide (WO_3) and porous titanium dioxide (TiO_2) films on AISI304 type steel were prepared by electrochemical methods. The morphology and structure of the obtained films were studied by X-ray diffraction analysis and scanning electron microscopy. Oxygen evolution catalyst containing cobalt–phosphate compound was deposited photochemically onto the surface of semiconductor particles. The photoelectrochemical properties of the prepared electrodes were investigated in neutral 0.1 M phosphate buffer solutions. The voltammetric characteristics revealed that the presence of cobalt-based catalyst effectively changes the photoelectrocatalytic activity of WO_3 and TiO_2 particles. The influence of some synthesis parameters (type of cobalt(II) salt, photodeposition time) on the electrochemical properties of the prepared electrodes was evaluated experimentally.

Key words: tungsten trioxide (WO_3), titanium dioxide (TiO_2), oxygen evolution catalyst, electrodeposition, photoelectrochemical

INTRODUCTION

The photoelectrochemical splitting of water into hydrogen and oxygen is considered as the very promising pathway in the development of a long-term, sustainable energy economy [1–4]. The realization of this process needs suitable catalytic materials which should fulfill strict technological requirements, such as stability over long periods of time, resistance to corrosion in aqueous solutions, ability to absorb a large portion of solar spectrum, promotion of oxygen and hydrogen evolution reactions. A multitude of materials have been tested for this purpose. Despite the considerable achievements, no cost-effective photoelectrochemical system was found to satisfy all requirements.

It is well established that the oxygen evolution reaction (OER) is a rate-limiting step of the overall water splitting process [5, 6]. It requires the removal of four protons and four electrons and the formation of the oxygen-oxygen double bond. It

is known that the OER always proceeds on oxidized surfaces. A rutile-type RuO_2 and IrO_2 have been identified to exhibit the lowest overpotential toward the OER. However, their practical use as electrocatalytic materials is hindered by the limited availability of ruthenium and iridium compounds in the Earth's crust. For these reasons, the efforts have been made in the search of OER catalyst based on earth-abundant elements [7]. In 2008, Nocera et al. [8] reported for the first time that the electrolysis of Co^{2+} salts in the neutral phosphate electrolyte using ITO electrodes leads to the formation of highly active water oxidation catalyst. The as-deposited cobalt–phosphate compound (termed Co–Pi) has been proved to be very active in neutral pH solutions [9–13]. It has been demonstrated that this catalyst, when coupled with semiconductors, can enhance the efficiency of photoelectrochemical water splitting [14–17]. Structural studies of cobalt–phosphate oxygen evolving catalyst suggest [10] that amorphous Co–Pi is composed of bis- μ -oxo/hydroxo-linked Co ions and support a molecular cobaltate cluster (MCC) model. According to this model the Co-oxo/hydroxo clusters possess the same structural motif

* Corresponding author. E-mail: simona.ostachaviciute@ktu.lt

found in the extended planes of cobaltates – edge sharing CoO₆ octahedra – but have molecular dimensions. It has been suggested that the molecular dimensions of the clusters found in Co–Pi may be essential for OER catalysis.

The aim of this work was to modify tungsten trioxide (WO₃) and titanium dioxide (TiO₂) films on AISI304 type stainless steel with cobalt-based OER catalyst and to study their structure and photoelectrochemical properties in aqueous solutions.

MATERIALS AND METHODS

Preparation of WO₃ and TiO₂ electrodes

WO₃ films on stainless steel were prepared by electrochemical deposition using a standard three electrode cell. AISI304 stainless steel plates 50 × 25 × 0.5 mm were used as a support. According to the manufacturer, the composition of stainless steel is as follows (wt. %): C, 0.08; Cr, 18–20; Ni, 8–10.5; Mn, 2.0; Si, 1.0; P, 0.045; S, 0.03; Fe, the remaining amount.

All solutions were prepared with doubly distilled water and analytical grade reagents. Sodium tungstate (Na₂WO₄ · 2H₂O, purity >99.7%) was obtained from Reachim (Russia) and used as received. The electrolyte itself was prepared according to the following procedure. First, sodium tungstate solution was mixed with hydrogen peroxide (H₂O₂, 30%, Lach-Ner, Czech Republic). Afterwards, nitric acid (HNO₃, 65%, Penta, Czech Republic) was added to the solution containing tungsten(VI)-peroxo complex. Only freshly prepared solutions were used for the measurements. All solutions were not deaerated during the experimental runs. All measurements were carried out at ambient temperature (291 K). The as-deposited samples were thermally treated under air atmosphere at 673 K for 1 h. The most uniform and stable films are obtained at –0.35 V after 20 min of electrolysis in 0.1 M Na₂WO₄ + 0.1 M H₂O₂ + 0.3 M HNO₃ electrolyte.

TiO₂ coatings on AISI304 type stainless steel were formed by electrophoretic deposition. A suspension for EPD was prepared by dispersing TiO₂ powder in methanol (purity 99.5%, Lachema, Czech Republic). A homogenous suspension was achieved under vigorous stirring for 10 min. Two stainless steel plates (50 × 25 × 0.5 mm each) were immersed into the prepared suspension of TiO₂. The distance between the anode and the cathode was 2 cm. EPD synthesis was performed under constant voltage (30 V) and was controlled using a DC power supply B5-49 (MNIPI Inc., Russia). The deposition time was varied from 1 to 3 min. For a better adhesion of TiO₂, all samples were thermally treated under an air atmosphere at 673 K for 1 hour.

Cobalt–phosphate catalyst (throughout the paper denoted as Co–Pi) was loaded on the surface of WO₃ and TiO₂ electrodes by a photochemical method. For this purpose, the photoanode was immersed in 0.1 M phosphate solution (pH 7) containing 0.5 mM Co(NO₃)₂ and illuminated for 5–40 minutes with a 400 W high pressure metal halogen lamp (Philips 400/30S).

Analytical techniques

The photoactivity of the prepared electrodes was investigated using photovoltammetric methods. The electrochemical measurements in the dark and under UV irradiation were performed by a computer-controlled Autolab PGSTAT12 (Ecochemie, The Netherlands) potentiostat / galvanostat. The GPES® 4.9 software was used for the collection and treatment of the experimental data. A two compartment photoelectrochemical quartz cell was employed. The electrolyte volume in each compartment was the same (100 mL). The anodic compartment contained WO₃ or TiO₂ coupled with Co–Pi catalyst as a working electrode and Ag, AgCl/KCl(sat) as a reference electrode. Throughout the paper all potentials are referred to this electrode. The cathodic compartment housed a platinum wire (geometric area about 15 cm²) as a counter electrode. 0.1 M potassium phosphate solution (pH 7) was used as a supporting electrolyte. The coated area of electrode was carefully positioned in the path of UV irradiation. A General Electric F8W/BLB lamp was placed at a distance of 2 cm from the WO₃ or TiO₂ electrode and was used as a UV radiation source. The lamp emits mainly in the 315–400 nm range, the peak wavelength λ_{max} being at 366 nm.

The X-ray powder diffraction (XRD) data were collected with a DRON-6 (Bourestnik Inc., Russia) powder diffractometer with Bragg-Brentano geometry using Ni-filtered CuK_α radiation and a graphite monochromator. The crystallite size D_{hkl} was calculated from the line broadening using the Scherrer's equation [18]:

$$D_{hkl} = \frac{k \cdot \lambda}{B_{hkl} \cdot \cos \Theta}$$

where λ is the wavelength of the Cu K_α radiation (1.54056 × 10⁻¹⁰ m), θ is the Bragg diffraction angle, B_{hkl} is the full width at the half maximum intensity of the characteristic reflection peak and k is a constant (the value used in this study was 0.94).

The rutile content in the TiO₂ coating was calculated according to the following equation [19]:

$$x = \left(1 + 0.8 \frac{I_A}{I_R} \right)^{-1}$$

where x is the weight fraction of rutile in the powder, I_A and I_R are intensities of the characteristic peaks of anatase (2θ = 27.5°) and rutile (2θ = 27.5°), respectively.

All scanning electron microscopy (SEM) images were acquired using Hitachi S-4800 or Quanta FEG scanning electron microscopes operating at 2 or 3 kV accelerating voltage.

RESULTS AND DISCUSSION

Structural and morphological characterization of WO₃ and TiO₂ electrodes

The amount of electrodeposited WO₃ was 1.3 ± 0.1 mg cm⁻², as determined by the gravimetric method. Assuming that the bulk density of WO₃ is 7.16 g cm⁻³ [20], the calculated average

thickness of these coatings is about 1.8 μm . XRD analysis reveals diffraction peaks corresponding to the crystalline WO_3 (Fig. 1, b). According to the Scherrer's equation, the average WO_3 crystallite size was calculated to be about 33 nm.

The amount of TiO_2 deposited was $0.7 \pm 0.1 \text{ mg cm}^{-2}$. Assuming that the bulk density of P25 TiO_2 is 3.8 g cm^{-3} [21], the approximate thickness of these TiO_2 coatings is 1.8 μm . The XRD pattern of the P25 TiO_2 powder on AISI304 stainless steel reveals the characteristic peaks of anatase and rutile at $2\theta = 25.4^\circ$ and 27.5° , respectively (Fig. 1a). The calculated values of crystallite sizes are 21 nm (anatase) and 54 nm (rutile). On the basis of these peak intensities, the rutile content in the TiO_2 electrode was calculated to be 27%. It should be noted that a detailed study of the structure and the morphol-

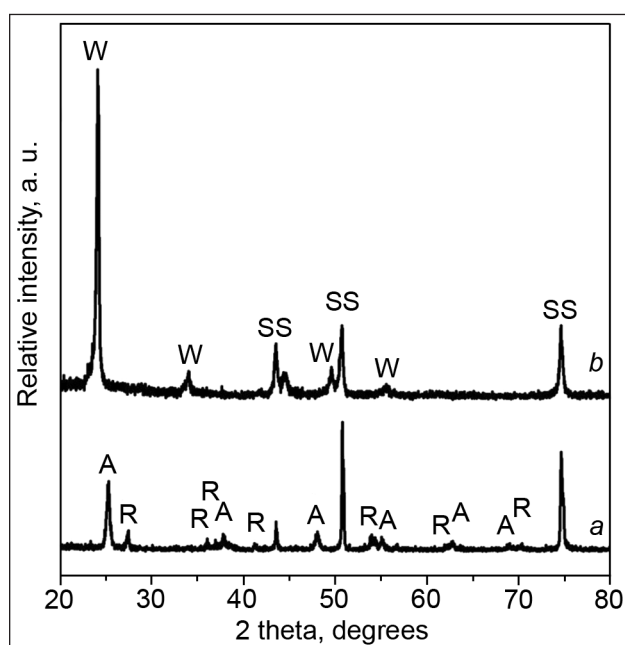
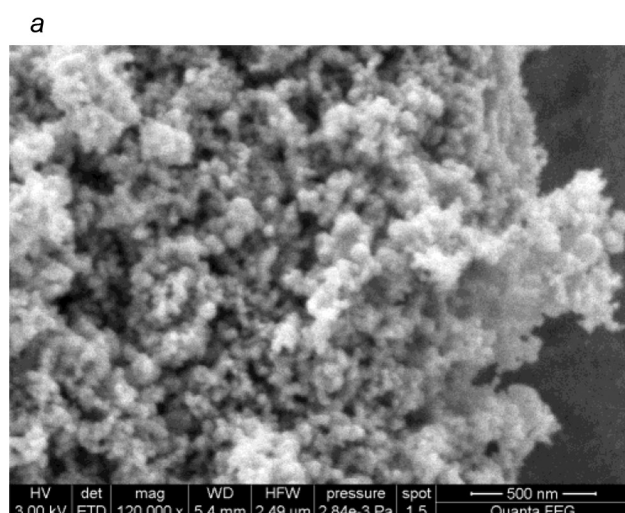


Fig. 1. XRD patterns of TiO_2 (a) and WO_3 (b) catalysts. Indexes: A – anatase, R – rutile, W – tungsten trioxide, SS – stainless steel



ogy of fresh P25 type TiO_2 revealed the coexistence of amorphous, anatase and rutile phases [22]. The authors suggested that the intimate contact between different phases results in the increase of the efficiency of electron-hole separation and this may account for the unusually large photocatalytic activity of this form of TiO_2 .

SEM images of the representative tungsten trioxide and titanium dioxide coatings are shown in Fig. 2. Continuous WO_3 coating consists of randomly positioned <50-nm particles in good agreement with XRD data. The analysis confirmed that nanoparticulate TiO_2 coatings are highly porous.

Photoelectrochemical properties of WO_3 and $\text{WO}_3/\text{Co-Pi}$ electrodes

The electrodeposited WO_3 films present n-type semiconductor behavior, as it is evidenced from current-potential curves obtained in the dark and under UV irradiation (Fig. 3). In the case of a continuous n-type semiconductor film, a depletion layer can be developed upon contact with the electrolyte which facilitates the separation of photogenerated holes and electrons. According to the Gartner-Butler model [23], the presence of the depletion layer can be determined by plotting the square of the photocurrent density with respect to the applied potential. The inset in Fig. 3 shows that the plot is linear in the rising part of the obtained photovoltammograms, thus, confirming the presence of the depletion layer in the prepared WO_3 films.

The linear sweep voltammograms of bare WO_3 and $\text{WO}_3/\text{Co-Pi}$ electrodes were recorded in order to study the catalytic effects of deposited cobalt-phosphate compound for electrochemical oxygen evolution in the dark (Fig. 4). The obtained experimental data show that the presence of Co-Pi catalyst shifts the onset potential for oxygen evolution by approximately 0.6 V. The increase in Co-Pi photodeposition time results in the increase in the onset potential shift. It means that higher amount of Co-Pi catalyst enhances the rate of oxygen evolution reaction. It can be suggested that at the photodepo-

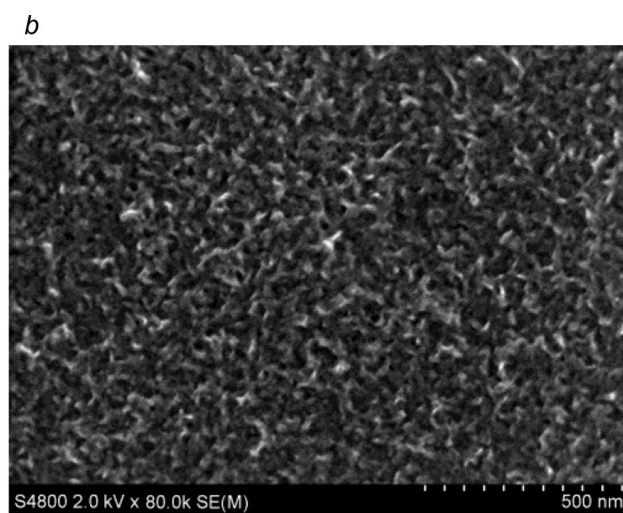


Fig. 2. Representative SEM images of TiO_2 (a) and WO_3 (b) films

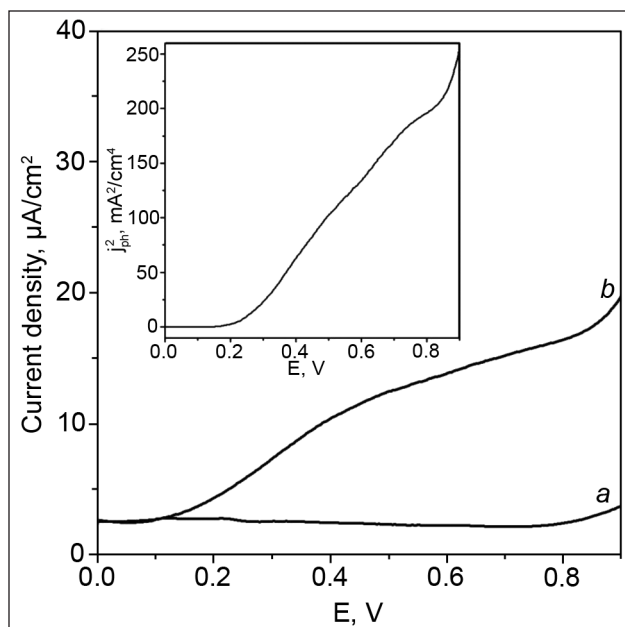


Fig. 3. Characteristic voltammograms in the dark (a) and under UV illumination (b) of the bare WO₃ electrode annealed at 673 K. Potential scan rate $v = 10 \text{ mV s}^{-1}$, 0.1 M phosphate buffer (pH 7). Inset: Plot of the square of the photocurrent density, j_{ph}^2 , with respect to the applied potential, E

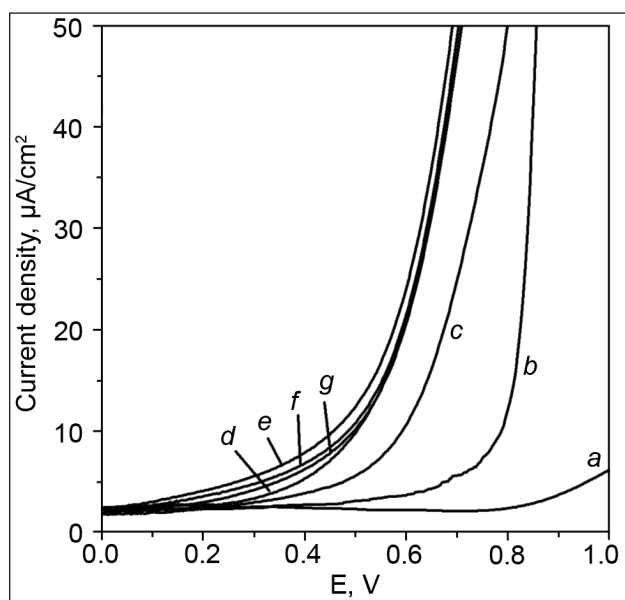


Fig. 4. Characteristic voltammograms in the dark of the bare WO₃ electrode (a) and WO₃ electrode coated with Co-Pi OEC for 10, 20, 30, 40, 50 and 60 min (b–g, respectively). Potential scan rate 10 mV s^{-1} , 0.1 M phosphate buffer (pH 7)

sition time longer than 30 min the continuous Co-Pi layer is formed on the surface of WO₃ as the anodic currents become steady (Fig. 4, curves d–g). A detailed characterization of the structure and composition of as-deposited WO₃/Co-Pi films is under investigation and the results will be published in a separate paper.

A mechanism of water splitting in the presence of Co-Pi oxygen evolution catalyst was proposed in [24]. The ex-

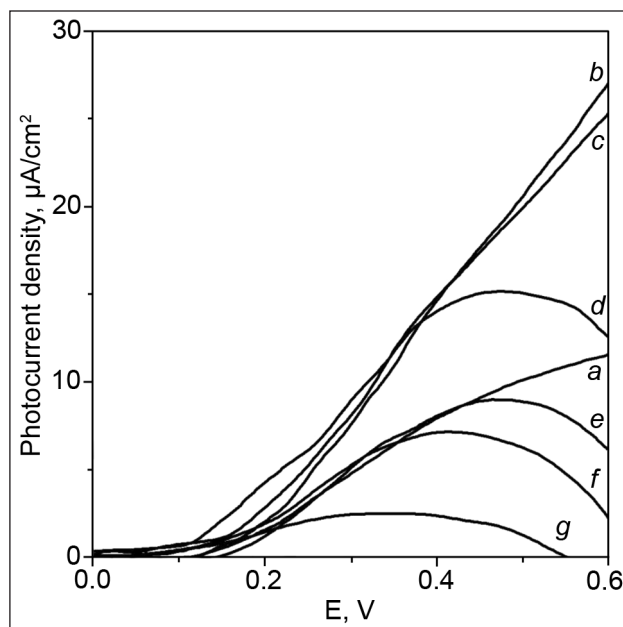


Fig. 5. Photocurrent density of the bare WO₃ electrode (a) and WO₃ electrode coated with Co-Pi OEC for 10, 20, 30, 40, 50 and 60 min (b–g, respectively). Potential scan rate 10 mV s^{-1} , 0.1 M phosphate buffer (pH 7)

perimental evidences show that the activation of oxygen in water involves a rapid one-electron, one-proton equilibrium between Co^{III}-OH and Co^{IV}-O in which a phosphate species play an essential role as a proton acceptor.

The photocurrent density dependences on the applied potential for WO₃ and WO₃/Co-Pi electrodes are presented in Fig. 5. It was established that at shorter Co-Pi photodeposition time the presence of the oxygen evolution catalyst enhances the observed photocurrents as compared to bare WO₃. However, at higher Co-Pi amounts the photocurrents are diminished.

The measurements show that the onset potential for the photocurrent of bare WO₃ is about 0.1 V. In the case of WO₃/Co-Pi films the photocurrent onset potential was shifted by approximately 0.08–0.12 V. This observation can be explained by assuming that the Co-Pi catalyst reduces the recombination rate near the flat-band potential region [16]. At higher potentials the particles of the Co-Pi catalyst act as recombination centers.

In order to investigate the stability of photocurrent in phosphate buffer over prolonged irradiation time, the chronoamperometric curves were recorded using bare WO₃ and WO₃/Co-Pi electrodes (Fig. 6). It was established that for both electrodes the photocurrents decline immediately within the first 2 min. Such a complex behavior of WO₃/Co-Pi films under UV irradiation is apparently due to the interplay of various processes occurring on the surface of the electrode. First of all, it should be noted that the chemical dissolution of WO₃ in the neutral solution takes place [25, 26]. Seabold and Choi [16] have shown that the chemical dissolution is not as severe as photodissolution. In addition,

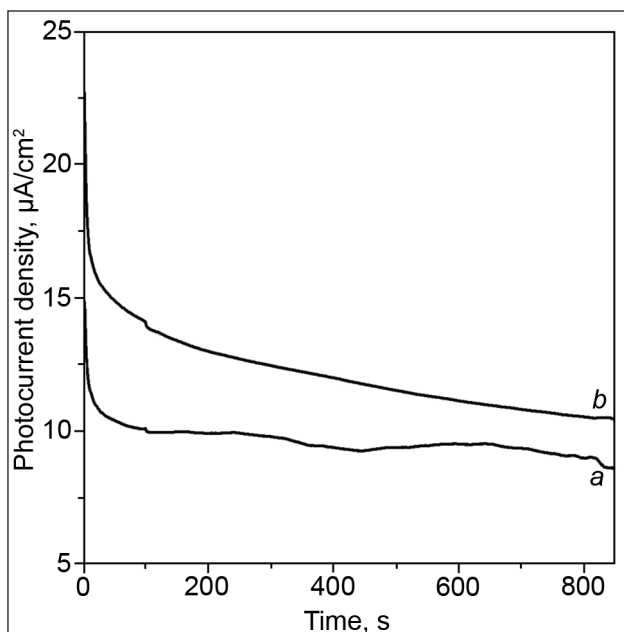


Fig. 6. Photocurrent profiles at +0.6 V bias for the bare WO_3 (a) and WO_3 electrodes coated with Co-Pi for 10 min (b)

the peroxy species are formed on the surface of WO_3 upon irradiation. The subsequent formation of tungsten-peroxy species leads to the loss of photoactivity. The dissolution rate induced by surface-bound peroxy species may be minimized by using acidic solutions. However, in the acidic medium the Co-Pi catalyst is unstable. On the other hand, the formation of peroxy species can be prevented by the presence of the Co-Pi catalyst. Thus, further research should be carried out in order to prepare a stable $\text{WO}_3/\text{Co-Pi}$ photoanode operating in a neutral electrolyte.

Photoelectrochemical behavior of TiO_2 and $\text{TiO}_2/\text{Co-Pi}$ electrodes

The photovoltammetry measurements confirmed (Fig. 7) that the prepared TiO_2 film acts as the n-type semiconductor electrode. It has been previously reported [27] that the space charge layer for the prepared P25 TiO_2 electrode is not formed and charge separation occurs via diffusion. In such nanoparticles the charge recombination is still a dominant process.

The time dependence of the open circuit potential of the bare TiO_2 electrode in the 0.1 M phosphate buffer is presented in the Inset of Fig. 7. One can see that in the dark the electrode has a potential of approximately -0.45 V. Under UV irradiation, the potential jumped negatively to about -0.62 V and reached a steady-state value. When the UV irradiation source was switched off, the potential started to increase. The decrease in the potential can be related to the fact that the photogenerated electrons accumulate and charge negatively the surface of TiO_2 particles. Photogenerated holes interact with water molecules which are present on the surface of TiO_2 [1, 2].

The presence of the cobalt-based oxygen evolution catalyst has an influence on the values of observed photocur-

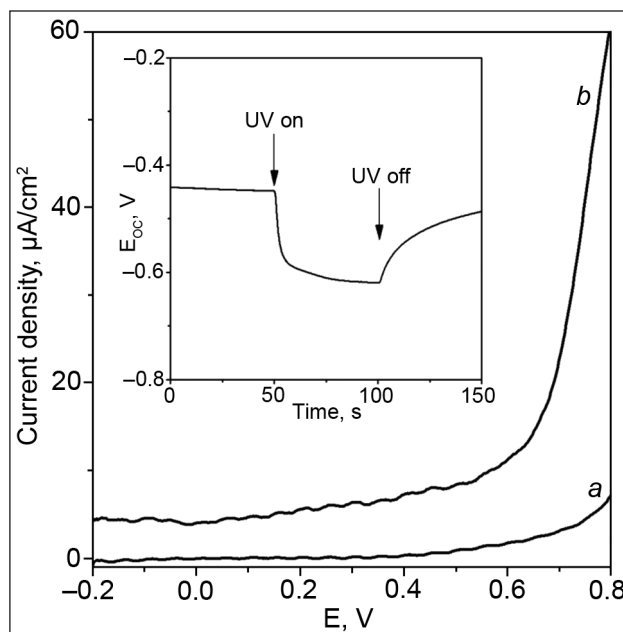


Fig. 7. Characteristic voltammograms in the dark (a) and under UV irradiation (b) of the bare TiO_2 electrode in 0.1 M phosphate buffer at 20 mV s^{-1} potential scan rate. Inset: Influence of UV light on the variation of open circuit potential E_{oc} in time

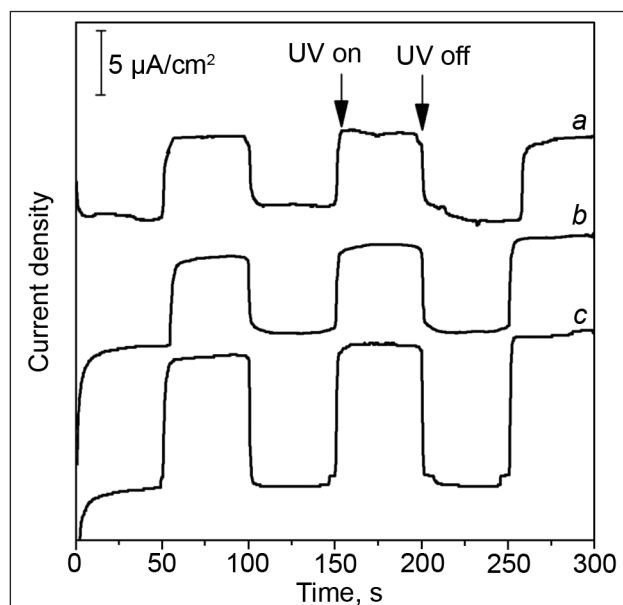


Fig. 8. Current density profiles at +0.2 V potential under chopped light conditions for the bare TiO_2 (a) and TiO_2 electrodes coated with Co-Pi for 10 min (b) or 15 min (c). Co-Pi catalyst photodeposited using 0.5 mM Co(II) nitrate solution

rents (Fig. 8). The highest photocurrents (about $10 \mu\text{A cm}^{-2}$) were obtained when the photodeposition of the Co-Pi catalyst onto the surface of TiO_2 lasted 15 min. At higher amounts of the deposited Co-Pi catalyst the photocurrents are diminished. Apparently, the Co-Pi catalyst increases the recombination rate of photogenerated charge carriers in TiO_2 particles.

In order to evaluate the influence of preparation conditions on the electrochemical properties of $\text{TiO}_2/\text{Co-Pi}$ elec-

trodes, three different cobalt(II) salts were used for the photodeposition of the Co–Pi catalyst. The photoactivity of the prepared $\text{TiO}_2/\text{Co–Pi}$ electrodes was compared by measuring the chronoamperometric transients at +0.2 V bias under UV irradiation and in the dark. The obtained experimental results revealed that the highest photocurrents can be obtained when cobalt(II) nitrate is used for the modification of the TiO_2 surface (Fig. 9). Cobalt(II) acetate and chloride were found to be less suitable for these purposes. The importance of cobalt(II) precursor is also confirmed by chronopotentiometric measurements (Fig. 10). Apparently, the presence of different anions in the electrolysis bath leads to the formation of Co–Pi layers having different structure and composition. However, a detailed structural characterization of such Co–Pi layers is needed in order to support this assumption. In addition, the influence of various cobalt(II) precursors on the electrochemical properties of $\text{WO}_3/\text{Co–Pi}$ electrodes will be studied.

CONCLUSIONS

Nanosized WO_3 and TiO_2 films on AISI304 type steel were prepared by electrochemical and electrophoretic deposition, respectively. The surface of oxide particles was modified with the cobalt–phosphate (Co–Pi) oxygen evolution catalyst in order to study its influence on the photovoltammetric characteristics of the electrodes. The obtained results show that the photo-assisted deposition of the Co–Pi catalyst significantly influences photoelectrochemical activity of both oxides. In the case of tungsten trioxide, the presence of the Co–Pi catalyst shifts the onset potential for O_2 evolution in the dark by approximately 0.6 V as compared to bare WO_3 . Similarly, the photocurrent onset potential was shifted by 0.1 V. It was determined that the optimum amount of the catalyst exists for the enhancement of photocurrents. Three different cobalt(II) salts (nitrate, acetate, chloride) were tested as precursors for the photo-assisted deposition of the Co–Pi catalyst on the surface of TiO_2 particles. The experimental data suggest that for this purpose the most suitable is cobalt(II) nitrate. However, a more detailed study of the structure and photoelectrochemical behavior of such composite films is needed, especially addressing the problem of photoanode stability.

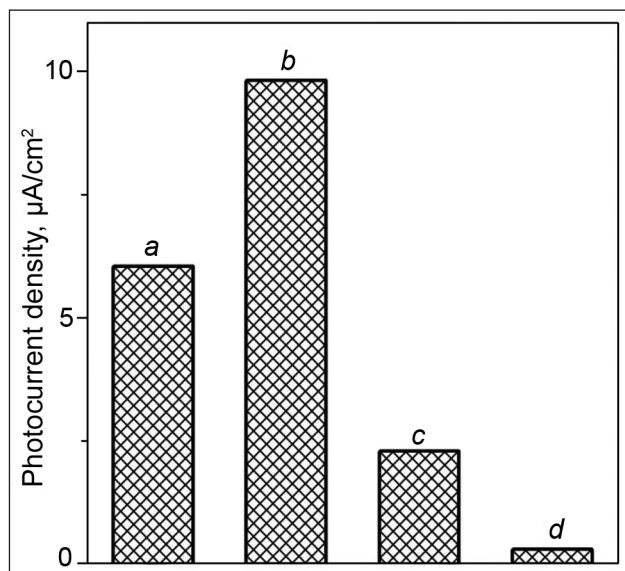


Fig. 9. Photocurrent density at +0.2 V potential of the bare TiO_2 (a) and $\text{TiO}_2/\text{Co–Pi}$ electrodes prepared using different 0.5 mM cobalt(II) salts: nitrate (b); acetate (c); chloride (d). 0.1 M phosphate buffer, Co–Pi photodeposition time 10 min

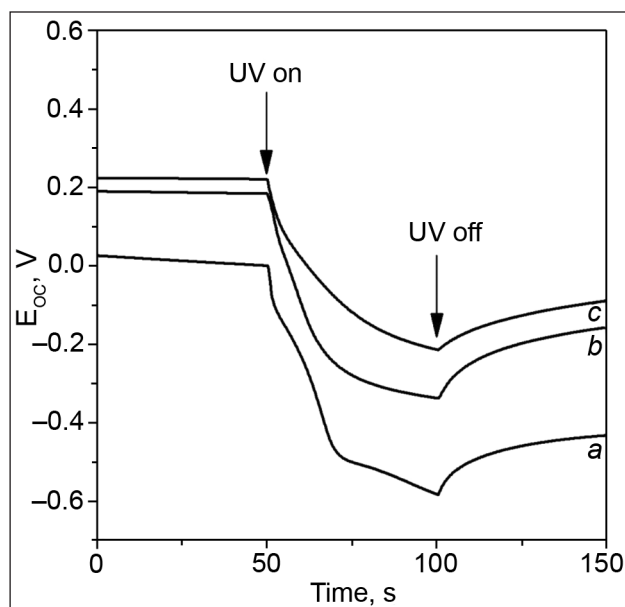


Fig. 10. Variation of the open circuit potential E_{oc} in the dark and under UV irradiation of the $\text{TiO}_2/\text{Co–Pi}$ electrodes prepared using different cobalt(II) salts: nitrate (b); acetate (c); chloride (d). 0.1 M phosphate buffer, Co–Pi photodeposition time 10 min

ACKNOWLEDGEMENTS

Rasa Mardosaitė acknowledges support by the project “Promotion of Student Scientific Activities” (VP1-3.1-ŠMM-01-V-02-003) from the Research Council of Lithuania. This project is funded by the Republic of Lithuania and European Social Fund under the 2007–2013 Human Resources Development Operational Programme’s Priority 3.

Received 12 March 2014

Accepted 13 May 2014

References

1. C. A. Grimes, O. K. Varghese, S. Ranjan, *Light, Water, Hydrogen. The Solar Generation of Hydrogen by Water Photoelectrolysis*. Springer Science+Business Media, LLC (2008).
2. R. van de Krol, M. Grätzel, *Photoelectrochemical Hydrogen Production*, Springer Science+Business Media, LLC (2012).
3. K. Rajeshwar, R. McConnell, S. Licht, *Solar Hydrogen Generation. Toward a Renewable Energy Future*, Springer Science+Business Media, LLC (2008).

4. J. R. McKone, N. S. Lewis, H. B. Gray, *Chem. Mater.*, **26**(1), 407 (2014).
5. I. Katsounaros, S. Cherevko, A. R. Zeradjanin, K. J. J. Mayrhofer, *Angew. Chem. Int. Edit.*, **53**(1), 102 (2014).
6. L. Trotochaud, S. W. Boettcher, *Scripta. Mater.*, **74**, 25 (2014).
7. P. Du, R. Eisenberg, *Energ. Environ. Sci.*, **5**(3), 6012 (2012).
8. M. W. Kanan, D. G. Nocera, *Science*, **321**(5892), 1072 (2008).
9. D. K. Bediako, C. Costentin, E. C. Jones, D. G. Nocera, J. M. Saveant, *J. Am. Chem. Soc.*, **135**(28), 10492 (2013).
10. M. W. Kanan, J. Yano, Y. Surendranath, et al., *J. Am. Chem. Soc.*, **132**(39), 13692 (2010).
11. Y. Surendranath, M. Dinca, D. G. Nocera, *J. Am. Chem. Soc.*, **131**(7), 2615 (2009).
12. Y. Surendranath, M. W. Kanan, D. G. Nocera, *J. Am. Chem. Soc.*, **132**(46), 16501 (2010).
13. Y. Surendranath, D. A. Lutterman, Y. Liu, D. G. Nocera, *J. Am. Chem. Soc.*, **134**(14), 6326 (2012).
14. R. S. Khnayzer, M. W. Mara, J. Huang, et al., *ACS Catal.*, **2**(10), 2150 (2012).
15. E. M. P. Steinmiller, K. S. Choi, *P. Natl. Acad. Sci. USA*, **106**(49), 20633 (2009).
16. J. A. Seabold, K. S. Choi, *Chem. Mater.*, **23**(5), 1105 (2011).
17. Q. Liu, Q. P. Chen, J. Bai, et al., *J. Solid State Electr.*, **18**(1), 157 (2014).
18. L. V. Azaroff, *Elements of X-Ray Crystallography*, McGraw-Hill, New York (1968).
19. R. A. Spurr, H. Myers, *Anal. Chem.*, **29** (1957).
20. C. G. Granqvist, *Sol. Energ. Mat. Sol. C*, **60**(3), 201 (2000).
21. M. Ettliger, *Technical Bulletin Pigments*, **56**, 8 (1984).
22. R. I. Bickley, T. Gonzalez-Carreno, J. S. Lees, L. Palmisano, R. J. D. Tilley, *J. Solid State Chem.*, **92**(1), 178 (1991).
23. K. Rajeshwar, in: A. J. Bard, M. Stratmann, S. Licht (eds.), *Encyclopedia of Electrochemistry*, Wiley-VCH, Weinheim (2002).
24. D. G. Nocera, *Accounts Chem. Res.*, **45**(5), 767 (2012).
25. J. Augustynski, R. Solarska, H. Hagemann, C. Santato, *P. Soc. Photo-Opt. Ins.*, **6340**, U140 (2006).
26. M. Gratzel, Y. Oosawa, *J. Chem. Soc., Chem. Commun.*, **24**, 1629 (1984).
27. E. Valatka, Z. Kulesius, *J. Appl. Electrochem.*, **37**(4), 415 (2007).

Simona Ostachavičiūtė, Rasa Mardosaitė, Eugenijus Valatka

WO₃ IR TiO₂ DANGŲ, MODIFIKUOTŲ KOBALTO TURINČIU DEGUONIES IŠSISKYRIMO KATALIZATORIUMI, FOTOELEKTROCHEMINĖ ELGSENA

Santrauka

Darbo metu elektrocheminiais metodais suformuotos WO₃ ir TiO₂ dangos, kurių struktūra ir morfologija charakterizuotos rentgeno spindulių difrakcinės analizės ir skenuojančios elektroninės mikroskopijos metodais. Atliktas WO₃ ir TiO₂ dangų ant nerūdijančio plieno modifikavimas kobalto turinčiu deguonies išsiskyrimo katalizatoriumi bei ištirtas dangų fotoelektrocheminis aktyvumas vandeniniuose tirpaluose. Puslaidininkinėms dangoms fotochemiškai modifikuoti naudotos įvairios kobalto(II) druskos – Co(NO₃)₂, Co(CH₃COO)₂, CoCl₂. Eksperimento būdu nustatyta, kad didžiausias aktyvumas būdingas katalizatoriui, paruoštam naudojant kobalto(II) nitratą. Tiriant dangų fotoelektrochemines savybes 0,1 mol/l fosfatiniame buferiniame tirpale (pH 7) pastebėtas modifikuotų oksidinių dangų fotoelektrocheminio aktyvumo padidėjimas, palyginti su nemodifikuotomis WO₃ ir TiO₂ dangomis. Nustatyta, kad egzistuoja optimalus kobalto katalizatoriaus kiekis. Tuo metu užfiksuotos didžiausios fotosrovių vertės.